Domain configurations of nanostructured Permalloy elements

R. D. Gomez,[a] T. V. Luu, and A. O. Pak
Laboratory for Physical Sciences, 8050 Greenmead Drive, College Park, Maryland 20740 and Department of Electrical Engineering, University of Maryland, College Park, Maryland 20742

K. J. Kirk and J. N. Chapman
Department of Physics and Astronomy, University of Glasgow, Glasgow G12 8QQ, United Kingdom

The magnetization distributions of an array of small NiFe elements were studied using Lorentz transmission electron microscopy (LTEM) and magnetic force microscopy (MFM). The dependence of the domain configurations at zero field as a function of the aspect ratio was observed using MFM, and confirms the earlier observations using LTEM. Comparison of the images of similar islands using both techniques elucidate the complementarity between the LTEM and MFM measurements which individually show different facets of the magnetization distributions on soft magnetic thin films. © *1999 American Institute of Physics.*
[S0021-8979(99)69308-2]

I. INTRODUCTION

Lorentz transmission electron microscopy (LTEM) is sensitive to the component of magnetic induction perpendicular to the electron beam, averaged along the electron trajectory,[1] while magnetic force microscopy (MFM) in its usual implementation is sensitive to the divergence of the surface magnetization.[2] In other words, LTEM has the capability of imaging magnetization distributions that do not produce stray fields and has limited capability to reveal detail on the sources of magnetic fields, while MFM is receptive mainly to the magnetization distributions that generate magnetic fields. The two techniques are thus to some extent complementary, and as has been suggested in the literature, it makes sense to use both techniques to fully reconstruct the complete magnetization distribution.[3] Microlithographed NiFe thin film elements are ideal samples because they are widely studied using a variety of techniques[4–9] and are relatively well known. They also have important technological applications in the areas of magnetic recording and sensing. However, despite the vast volume of work on these elements, a direct comparison of MFM and TEM measurements on identical samples has yet to be reported.

This work is an attempt to explore the relationship between MFM and magnetic TEM images by studying a set of identical arrays of micron and submicron NiFe islands. Since NiFe islands have been studied extensively with LTEM, we will first discuss the domain configuration as observed using the MFM and confirm the dependence with the aspect ratio (AR). We will subsequently focus on several representative cases which highlight the relationship between the two imaging techniques.

II. EXPERIMENTS

The samples were prepared by electron beam lithography and lift-off patterning on electron transparent Si_3Ni_4 membrane substrates for LTEM and solid substrates for MFM. A 26 nm thick layer of NiFe alloy ($B_s = 1.2$ T) was deposited by thermal evaporation. The samples were imaged in the TEM in Fresnel, Foucault, and differential phase contrast (DPC) modes, both in the remanent state and in an applied field during *in situ* magnetizing experiments. The topography and magnetic features of the islands on solid substrates were simultaneously imaged using a commercial (Nanoscope Multimode) MFM, with the probe premagnetized along the vertical direction. A low moment probe was used at a lift height of 50 nm to minimize the measurement-induced domain wall motion.

III. RESULTS AND DISCUSSION

A. Aspect ratio and domain configuration

Figure 1 shows the MFM image of the NiFe array, and the remanent configurations of the individual islands after applying roughly 150 Oe in-plane magnetic field in the direction shown by the arrow. The dimensions of the sides are indicated at the borders and also serve as convenient indices to identify specific islands. We adopt the labeling convention (R,C) indicating the row and column dimensions. The islands were arranged so that every off-diagonal element would have a transpose oriented in the orthogonal direction and the diagonal elements, of course, all have aspect ratios of 1. Despite the large range and variation in aspect ratios, the patterns exhibit only a few types of unique configurations, namely:

(A) four domain closure pattern with four 90° walls,
(B) seven domain closure pattern,
(C) four domain closure with four 90° and one 180° wall,
(D) four domain wall pattern with cross-tie and Bloch line inclusion along the 180° wall,
(E) quasisingle domain with flux closure ends,
(F) single domain with unresolved localized end structure,
(M) complex multidomain state.

Types A–D possess no net moment at remanence or solenoidal. We use the above classification to survey the relationship between the aspect ratio and domain configuration. Most, but not all, diagonal elements form the type A pattern even down to the smallest element ($0.5\times0.5\ \mu m^2$). The exceptions are the largest islands: the 3 μm shows a type

[a]Electronic mail: rdgomez@glue.umd.edu

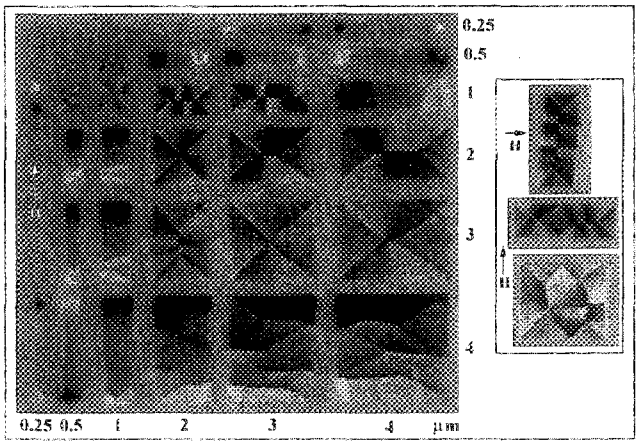

FIG. 1. Magnetic force microscope images of an array of Permalloy islands at remanence. A 150 Oe external field along the direction indicated by the arrow was applied prior to imaging.

B—seven domain configuration shown on the bottom inset—and the 4 μm square shows a type M—nonsolenoidal, with curved interior domain walls. The former pattern was observed in the as-deposited state as well as in some experimental runs involving various magnetizing cycles, and it is consistent with previous reports on similar islands.[7] (Another interesting variation of type B is shown in the 3×1 μm^2 island in the middle inset). The latter type M configuration appears intermittently after saturating the element along one of its easy axes and returning the field to zero. These islands often revert to the type A pattern after an application of less than 5 Oe field in the reverse direction. The type A configuration is retained even as the aspect ratio deviates from 1,

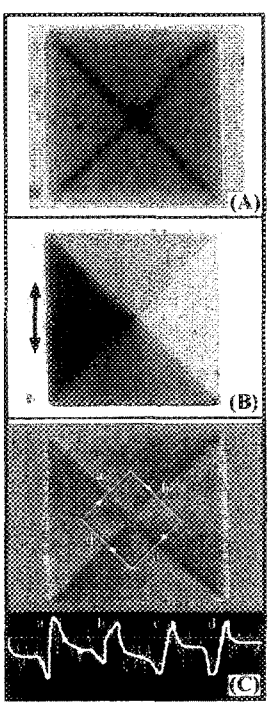

FIG. 2. The TEM and MFM images of square NiFe islands at zero field, showing the closure pattern formed 90° domain walls: (a) Fresnel image and (b) Foucault image of a 2×2 μm^2 island, and (c) MFM image of a 3×3 μm^2 island.

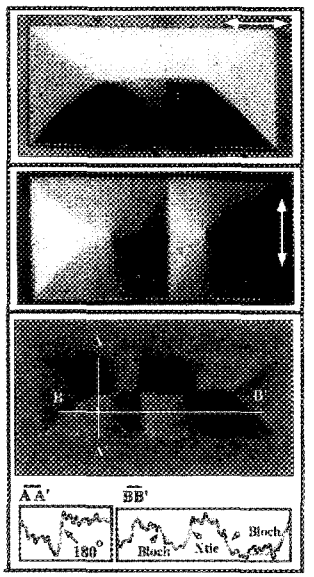

FIG. 3. The TEM and MFM images of rectangular islands at zero field showing the closure pattern formed by 90° and 180° walls with crossties: (a) and (b) Foucault images of a 2×1 μm^2 island with a crosstie in the 180° wall and Bloch lines at the points of the triangular domains and (c) MFM image of a $3\times1\times0.02$ μm^2 rectangular island at zero field showing two Bloch lines in the 180° wall and one crosstie near the center.

and as typified by Is(3,4)(AR=1.33), a slight wall curvature is introduced to compensate the departure from geometrical squareness while maintaining the convergence of the walls into a single point. Curved domain walls become energetically costlier with increasing AR, so that at the aspect ratio of 1.5, Is(2,3), the type C configuration becomes more favorable. The type C is favorable up to AR=2, but becomes degenerate with the type D configuration. As typified by Is(1,2), type D differs from type C due to the formation on a crosstie on the 180° wall. Variations of the type D pattern were also evident in some islands. As illustrated in the inset, 1×3 μm^2 (top) island shows three crossties and four Bloch lines. Nevertheless, the type D pattern appears to be energetically favorable up to AR=3[Is(1,3)], and beyond which the islands change from solenoidal to the nonsolenoidal. The first nonsolenoidal configuration is the type E which is best seen in Is(1,4). The featureless central region indicates a uniform magnetization parallel to the easy axis. The fine structures at the opposite ends are multidomains which diminish

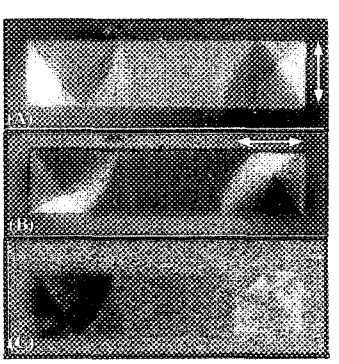

FIG. 4. Foucault TEM images and MFM images of a 4×1 μm^2 island showing the multidomain end regions.

as the island width is reduced. At the aspect ratio of 12, Is(0.250, 3), the fine structures are no longer visible and end regions appear only as a pair of highly localized magnetic charges, classified as single domain, type F configuration.

The direction of the field is influential is establishing the remanent domain configurations. Details of this are beyond the scope of this short article but is discussed elsewhere.[15] Briefly, however, we see that the elements below the diagonal—those islands which were exposed to the field along their easy axes—favor a nonsolenoidal configuration much more readily than the ones above the diagonal. For instance, whereas islands (3,4) exhibits a type A closure domain, the island (4,3) exhibits the complex structure, type M, but with localized charges at the ends. The same distinction can be said between (2,4) and (4,2), and so on. Finally, we note the energy differences between configurations is very small so that it is possible to observe a given island in several different magnetization distributions.

B. Domain wall imaging using MFM and TEM

Figure 2 shows both TEM and MFM images of a square ing 90° domain walls and a central vortex. The Foucault image in Fig. 2(b) maps the component of induction in the direction indicated by the arrow. The MFM image in Fig. 2(c) is complementary with the TEM images, and provides additional information on the charge distribution in the walls and in the domains themselves. The line profile shown below the MFM image was extracted along the indicated circuit starting from the lower left wall and proceeding clockwise. The bold lines are averaged over many scan lines while the faint line is a representative single profile to provide a measure of the noise level in measurements. The profile shows a slowly varying contour in the domains interrupted by rapid fluctuations across the 90° walls. The transition length at the walls, measured as the lateral distance between the dip and peak, is about 55 nm with an uncertainty of 5 nm. Such a profile is reminiscent of a dipolar magnetization distribution,[10] and one can regard the Néel wall formed by the intersecting 90° domains as a dipole layer with an upper limit of 55 nm width. Since the MFM is sensitive to the magnetic charge densities, we conclude that in the interior regions of the domains there is a small variation in magnetic charge corresponding to the long tails of the Néel walls.[11]

We now consider the case with 180° walls with Bloch lines and crosstie. Starting from the LTEM results, Figs. 3(a) and 3(b) are the Foucault images of a 2×1 μm^2 island with a crosstie and two Bloch lines. The magnetic induction is mapped in two orthogonal directions shown by the arrows. The contrast shows that a transverse component of the magnetization is present near the vicinity of the crosstie.[12] Figure 3(c) shows a MFM image for a 3×1 μm^2 rectangular element, also with a crosstie and two Bloch lines, although in this case the Bloch lines are displaced along the 180° wall. Across the 180° wall (along segment AA′) the profile exhibits a depression followed by a peak and a distinctive step function. The measured transition length is about 55 nm, the same as in the 90° wall, which could indicate some instrumental resolution limit since the 180° wall is expected to be narrower.[13,14] The variation of the interior contrast of the top and bottom trapezoids implies that the magnetization is nonuniform in those regions. The alternation of bright–dark contrast is associated with Bloch lines and crossties, as shown in the profile BB′.

Finally, we consider the characteristics of the edge domains in the nonsolenoidal pattern of Fig. 4. This 4×1 μm^2 island shows the characteristic end structures first observed by McVitie and Chapman.[8] The MFM images show that while fine subdomainlike features exist in the end regions, the general contrast is dark on one end and bright on the other. This implies that net positive or negative charges are localized at the end regions in the form of $-\mathrm{div}^*\mathbf{M}$. Since the intensity is proportional to the change in magnetization, then the magnetization in the interior of each of the subdomains is nonuniform and varies to induce positive (or negative) magnetic charges. The effect is especially pronounced in three out of the four domains and somewhat subdued in the fourth one. The fourth subdomain with weak contrast is uncharged and can be regarded as a uniformly magnetized. From the Foucault images, the direction of the magnetization of the subdomains are readily discerned. For this nonsolenoidal configuration, stray fields are also visible in the free space around the elements as dark or light shade depending on the direction.

In conclusion, both techniques reveal different facets of the magnetization distribution. LTEM offers the major advantage that the measurement process does not alter the magnetization state of the sample. MFM, on the other hand, uses the interaction force between the sample and probe and thus more prone to instrument-induced perturbations. However, the present results on a relatively soft ferromagnet and the excellent agreement between the two techniques shows that it is possible to achieve MFM results without significant perturbations to the sample magnetization. This is an important finding about MFM measurements and its use in soft thin films.

ACKNOWLEDGMENTS

This work was partially supported by the University of Maryland NSF MRSEC. The authors acknowledge the invaluable assistance of Dr. C. Kraft in manuscript preparation. This is dedicated to the memory of Dr. Edward R. Burke, a magnetician and a friend.

[1] D. R. Fredkin and S. Strikman, IEEE Trans. Magn. **24**, 2105 (1988).
[2] R. D. Gomez *et al.* J. Appl. Phys. **78**, 6441 (1996).
[3] I. A. Beardsley, IEEE Trans. Magn. **25**, 671 (1989).
[4] P. Grutter, H. J. Mamin, and D. Rugar, in *Scanning Tunneling Microscopy II*; 1st ed., edited by R. Wiesendanger and H.-J. Gunterodt (Springer, Berlin, 1992), Vol. 28, pp. 151–207.
[5] H. J. Mamin *et al.*, Appl. Phys. Lett. **55**, 318 (1989).
[6] G. A. Gibson *et al.*, IEEE Trans. Magn. **27**, 5187 (1991).
[7] K. Runge *et al.*, J. Appl. Phys. **79**, 5075 (1996).
[8] S. McVitie and J. Chapman, IEEE Trans. Magn. **24**, 1778 (1988).
[9] A. B. Johnston *et al.*, J. Phys. D **29**, 1419 (1996).
[10] R. Madabhushi, IEEE Trans. Magn. **32**, 4147 (1996).
[11] A. Hubert *et al.*, Phys. Status Solidi B **204**, 817 (1997).
[12] R. Ploessel *et al.*, J. Appl. Phys. **73**, 2447 (1993).
[13] A. Hubert, Phys. Status Solidi **38**, 699 (1970).
[14] S. McVitie and J. N. Chapman, J. Magn. Magn. Mater. **83**, 97 (1990).
[15] R. D. Gomez *et al.*, J. Appl. Phys. (these proceedings).